Regular Article

Ab initio molecular dynamics studies of Au$_{38}$(SR)$_{24}$ isomers under heating[⋆,⋆⋆]

Rosalba Juarez-Mosqueda[1,a], Sami Malola[1], and Hannu Häkkinen[1,2]

[1] Department of Physics, Nanoscience Center, University of Jyväskylä, 40014 Jyväskylä, Finland
[2] Department of Chemistry, Nanoscience Center, University of Jyväskylä, 40014 Jyväskylä, Finland

Abstract. Despite the great success in achieving monodispersity for a great number of monolayer-protected clusters, to date little is known about the dynamics of these ultra-small metal systems, their decomposition mechanisms, and the energy that separates their structural isomers. In this work, we use density functional theory (DFT) to calculate and compare the ground state energy and the Born-Oppenheimer molecular dynamics of two well-known Au$_{38}$(SCH$_2$CH$_2$Ph)$_{24}$ nanocluster isomers. The aim is to shed light on the energy difference between the two clusters isomers and analyze their decomposition mechanisms triggered by high temperatures. The results demonstrate that the energy that separates the two isomers is of the same order of magnitude as the energy difference between the *fcc* and *hcp* phases of bulk gold reported earlier. Moreover, the MD simulations show disordering and eventual fragmentation of the cluster structures at high temperature which seem to proceed via spontaneous formation of Au$_x$(SR)$_y$ polymeric chains. Hence, these results greatly contribute to understanding the possible decomposition mechanism, stability and robustness of existing and new monolayer-protected clusters.

1 Introduction

Since the first reports on thiolate-passivated gold clusters [1–4], about hundred atomically precise monolayer-protected nanoclusters (MPC) have been synthesized with highly reproducible physical properties [5–8]. Despite this great success, however, over the last few years of research in the field the latent question regarding the stability and robustness of this type of ultra-small systems has become critical. Many of the existing MPC have been observed to decompose over a period of several days as consequence of atomic re-organizations or core-size conversion triggered during manipulations, synthesis, or by effect of the environmental conditions [9–15]. Moreover, high-resolution electron microscopy studies have revealed that the exposure to normal electron dose inflicts significant morphological and structural changes in ultra-small metal nanoparticles and nanoclusters [16–23]. All these structural changes occurring in the structure of MPC, especially in solution phase, often lead to coexistence of different chemical species that might hinder the crystallization

and the characterization of the main product, limiting thus their usage in practical applications [24,25].

In the particular case of Au$_{38}$(SR)$_{24}$ nanocluster, it took over a decade to experimentally disentangle the atomic structure [26–33]. In 2010, Qian et al. found through X-ray crystallography experiments that the metal core of the Au$_{38}$(SCH$_2$CH$_2$Ph)$_{24}$ nanocluster is a prolate biicosahedral with quasi-D_{3h} symmetry [33]. However, more recently Tian and co-workers have found, also by using single-crystal X ray crystallography, that the metal core of Au$_{38}$(SCH$_2$CH$_2$Ph)$_{24}$ nanoclusters can also adopt an oblate structure with relatively high stability at low temperatures [34]. They observed that the prolate structure reported by Qian [33] and Lopez-Acevedo [31] can irreversibly be obtained from this less symmetric oblate Au$_{38}$(SCH$_2$CH$_2$Ph)$_{24}$ cluster by heating the samples to 50 °C in toluene [34]. To date, this discovery is one in the large list of experimental data that underline the dynamical behavior of MPCs [9–13]. In spite of this, there is only a limited number of theoretical studies that focus on the dynamic behavior of MPC and that compare their energy with respect to structural isomers [35].

In this work, we used the Au$_{38}$(SCH$_2$CH$_2$Ph)$_{24}$ structures of Qian and Tian (hereafter denoted as Au$_{38Q}$ and Au$_{38T}$, respectively) as reference systems to compare the ground state energies, electronic structures, and dynamics of ligand-protected metal nanoclusters with same chemical composition. The aim is to shed light on the energy that separates these molecule-like isomers in their ground state

---

and to study the dynamics of both systems with increasing the temperature. For this purpose, we calculated the energy difference between the two isomers by using different approximations to the exchange-correlation energy in DFT calculations and we performed DFT molecular dynamics simulations from 0–1100 K to analyze the structural changes induced by high temperatures. We found that, in accordance with the experimental observations, the Au_{38T} nanocluster is less stable than the Au_{38Q}, and that the lower stability of the structure of Tian can be largely attributed to a combined effect of high fluxionality of the Au atoms and the weakness of specific Au–S bonds when exposed to heat. Furthermore, the MD simulations provide a possible mechanism by which the clusters start to disorder and finally fragment.

2 Computational methods

Structure optimizations, energy calculations, and electronic structure analysis were carried out using the density functional theory (DFT) as implemented in GPAW [36,37] code package. The electron density was modeled using a real-space grid with spacing of 0.2 Å. The structure optimizations were performed using a convergence criterion of 0.05 eV/Å for the residual forces on the atoms. The local-density approximation (LDA) [38], Perdew-Burke-Ernzerhof (PBE) [39], and van der Waals (vdW-DF-cx) [40,41] functionals were used to compare the total energy and the HOMO-LUMO energy gaps. In all-electron calculations, the $Au(5d^{10}6s^1)$, and $S(3s^23p^4)$, $C(2s^22p^2)$, and $H(1s^1)$ electrons were treated as valence and the innermost ones were included as a frozen core. The structure optimizations were performed using the $Au_{38}(SCH_2CH_2Ph)_{24}$ crystal structures of Tian [34] and Qian [31,33], as well as the corresponding simplified $Au_{38}(SCH_3)_{24}$ models (hereafter denoted as Au_{38t} and Au_{38q} for Tian and Qian structures, respectively).

Born-Oppenheimer NVT molecular dynamics (MD) simulations were performed on the optimized Au_{38t} and Au_{38q} structures by using the PBE exchange-correlation functional. The atomic mass of the hydrogen atoms was replaced by the mass of deuterium in order to use simulation time step of 2.0 fs. For comparison, a short MD simulation on the Au_{38t} structure was also performed using a time step of 1.0 fs to validate the dynamics observed with larger time step (see Figs. S3–S4 in Supplementary material). To equilibrate the systems the Berendsen thermostat was used with a coupling constant to the bath of $\tau = 0.5$ ps [42]. Initially, the MD simulations were performed at 500 K for 12 ps and 15 ps for Au_{38q} and Au_{38t}, respectively. However, to see more severe structural changes, the temperature was increased in steps of 100 K until it reached ~1100 K. The total simulation time was 24.768 ps for both clusters.

3 Results and discussion

In Figure 1, we show the Au_{38T} and Au_{38Q} structures optimized with PBE functional [39]. Both clusters consist of a Au_{23} core protected by a surface layer formed of
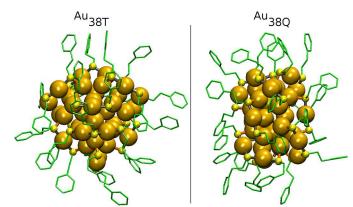

Fig. 1. Atomic structures of the $Au_{38}(SCH_2CH_2Ph)_{24}$ nanoclusters reported by Tian (Au_{38T}) and Qian (Au_{38Q}). The eighteen Au–S bonds formed between Au atoms of the Au_{23} core and S atoms (Au_{core}–S) are in orange. In gray, the thirty Au–S bonds within the $Au_n(SCH_2CH_2Ph)_m$ units (Au_{units}–S). The aromatic CH_2CH_2Ph groups are in green. The structures are optimized using the PBE functional.

several $Au_n(SCH_2CH_2Ph)_m$ units (with $n = 0, 1, 2,$ or 3, and $m = 1, 2, 3,$ or 4). In the Au_{38Q} cluster, the Au_{23} core is a biicosahedral structure with D_3 symmetry protected by six $Au_2(SCH_2CH_2Ph)_3$ and three $Au(SCH_2CH_2Ph)_2$ units. In the Au_{38T} isomer, the Au_{23} core is formed by one Au_{13} icosahedron and one Au_{12} cap (fused together via sharing two gold atoms), and the protecting layer consists of three $Au_2(SCH_2CH_2Ph)_3$, three $Au(SCH_2CH_2Ph)_2$, two $Au_3(SCH_2CH_2Ph)_4$ and one SCH_2CH_2Ph bridge. According to the superatom electron count formula, $n^* = Nv - M - z$ [43], from which the number of delocalized electrons in a core of the $Au_{38}(SR)_{24}$ clusters (n^*) is calculated as the product of the number of core metal atoms ($N = 38$) and their atomic valence ($v = 1$), minus the number of electron-withdrawing ligands ($M = 24$) and the overall charge ($z = 0$), these clusters have 14 delocalized electrons [31].

To reduce the computational burden in simulations we replace the SCH_2CH_2Ph ligands in the Au_{38Q} and Au_{38T} structures with SCH_3. To validate the choice of the $Au_{38}(SCH_3)_{24}$ (Au_{38q} and Au_{38t}) models, we calculate the density of states (DOS) of the Au_{38Q} and Au_{38T} clusters and compare them with the DOS of the simplified Au_{38q} and Au_{38t} structures. Figure 2 shows that the DOS of the $Au_{38}(SCH_2CH_2Ph)_{24}$ clusters match the DOS of the $Au_{38}(SCH_3)_{24}$ models within the energy range of -1.5 to 2.0 eV. This indicates that the states near the Fermi level are predominantly of the metal core and that the discrepancies outside the -1.5 to 2.0 eV energy window are due to the lack of the $\pi-\pi^*$ states of the phenyl rings in the ligands of the Au_{38q} and Au_{38t} structures.

Similarly, we investigate the effect of the ligands on the length of the chemical bonds by comparing the optimized Au–Au and Au–S bond distances between the Au_{38Q} and Au_{38q} structures. The results from the PBE calculations (shown in Tab. S1 in SI) demonstrate that the Au–Au bonds within the Au_{23} core (Au_{core}–Au_{core}), the Au-S bonds between Au atoms of the Au_{23} core and S (Au_{core}–S), and the Au–S bonds within the units

Table 1. Relative energies, E_r, HOMO–LUMO gaps (in parenthesis), and moments of inertia I_x, I_y and I_z (in square brackets) of the optimized $Au_{38}(SR)_{24}$ nanoclusters with $R = CH_3$ (Au_{38t} and Au_{38q}) and $R = CH_2CH_2Ph$ (Au_{38T} and Au_{38Q}). Energies, given in eV per cluster, are calculated using the LDA, PBE and vdW-DF-cx functionals. The moments of inertia are in units of 10^3 amu $Å^2$.

| | | $Au_{38}(SCH_3)_{24}$ | | $Au_{38}(SCH_2CH_2Ph)_{24}$ | |
		Au_{38t}	Au_{38q}	Au_{38T}	Au_{38Q}
LDA	E_r	0.43	0.00	2.14	0.00
	HOMO–LUMO	(0.83)	(0.95)	(0.81)	(0.86)
	I_x, I_y, I_z	[121, 123, 170]	[100, 158, 158]	[252, 271, 326]	[210, 312, 319]
PBE	E_r	0.34	0.00	1.76	0.00
	HOMO–LUMO	(0.85)	(0.92)	(0.88)	(0.88)
	I_x, I_y, I_z	[131, 134, 185]	[108, 170, 171]	[272, 292, 356]	[230, 334, 343]
vdW-DF-cx	E_r	0.45	0.00	3.14	0.00
	HOMO–LUMO	(0.85)	(0.93)	(0.82)	(0.90)
	I_x, I_y, I_z	[127, 130, 179]	[104, 166, 166]	[264, 283, 342]	[220, 325, 332]

(Au_{units}–S), have in average the same length in the Au_{38Q} and Au_{38q} structures (2.87 Å, 2.42 Å, and 2.34 Å). This indicates that replacing the true SCH_2CH_2Ph ligands with SCH_3 does not significantly affect the length of the Au–Au and Au–S bonds which, in turn, also reaffirms the validity of using the $Au_{38}(SCH_3)_{24}$ models. Moreover, the averaged bond lengths of the Au_{38Q} and Au_{38q} structures optimized with the vdW-DF-cx functional are very similar to the ones from PBE calculations, with a maximum difference of only 0.02 Å. In the crystal structure reported by Qian et al. [33], the averaged bond length of Au_{core}–Au_{core}, Au_{core}–S, and Au_{units}–S are 2.87 Å, 2.37 Å, and 2.30 Å, respectively (see Tab. S1 in Supplementary material).

In Table 1, we show the relative energies of the Au_{38Q} (Au_{38q}) and Au_{38T} (Au_{38t}) clusters calculated using different exchange-correlation functionals. The results confirm the highest stability of the Au_{38Q} structure over the Au_{38T} isomer by 1.8–3.1 eV (i.e., 3.7–6.7 meV per atom). The largest energy difference between these two crystal structures is obtained when using the vdW-DF-cx functional which accounts for long-range correlations that give rise to the vdW forces. These results importantly indicate that the effect of the van der Waals interactions is in the range of 1.0 to 1.4 eV. Moreover, when we calculate the ground-state energy of the simplified $Au_{38}(SCH_3)_{24}$ structures the energy difference between the Qian and Tian clusters drops to 0.3–0.4 eV per cluster (i.e., 2.1–2.8 meV per atom), indicating also that ~80% of the stabilizing energy of the Au_{38Q} nanocluster comes from the disposition of the SCH_2CH_2Ph ligands around the metal core.

Earlier, Wang et al. [44] reported that the energy difference between *fcc* and *hcp* phases of gold calculated using DFT/PW91 is 1.9 meV per atom. Comparing the results of Wang et al. with ours we find that the energy difference between the two forms of $Au_{38}(SR)_{24}$ are of the same order of magnitude as the energy difference between the *fcc* phase and the metastable *hcp* phase of bulk gold. Moreover, the phase transition of square sheets of *hcp* gold, of length of 200–500 nm and thickness of ~2.4 nm,
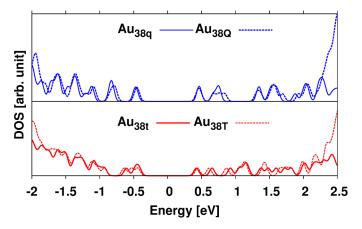

Fig. 2. Comparison of the density of states between the $Au_{38}(SCH_3)_{24}$ (Au_{38q} and Au_{38t}) and $Au_{38}(SCH_2CH_2Ph)_{24}$ (Au_{38Q} and Au_{38T}) structures. DOS are calculated by using the PBE functional.

to a *fcc* structure has been observed on exposure to an electron beam [45].

Also, in Table 1 we show the values of the HOMO–LUMO gap and the Cartesian moments of inertia, I_x, I_y, and I_z, of the optimized Au_{38T} and Au_{38Q}, and Au_{38t} and Au_{38q} structures. The corresponding oblate and prolate shape of the Au_{38T} (and Au_{38t}) and Au_{38Q} (and Au_{38q}) is confirmed by the $I_z > I_x \approx I_y$ and $I_z \approx I_y > I_x$ values, respectively. In general, the calculated HOMO–LUMO energy gap of the Au_{38Q} (and Au_{38q}) nanocluster is slightly larger than the one of the Au_{38T} (Au_{38t}) isomer. A HOMO–LUMO gap of 0.9 eV has been reported for the $Au_{38}(SR)_{24}$ species [31,46–48].

To describe the structural changes induced by heat on the two clusters isomers, we performed MD simulations using the Au_{38t} and Au_{38q} models. As expressed above, the resulting energy values from the local optimizations demonstrate that the disposition of the aromatic ligands around the metal core and the vdW interactions are important in stabilizing the two isomers (particularly in the case of Au_{38Q}). However, the use of the

simplified models in the MD simulations also provides important insights regarding the stability and robustness of the thiolate-protected metal structures in these two geometric arrangements, while it significantly reduces the computational burden.

In Figure 3, we show the optimized Au_{38t} and Au_{38q} structures (Figs. 3a and 3e) and different snapshots taken during the MD simulations which were performed using a time step of 2 fs (Figs. 3b, 3c, 3d, 3f, 3g and 3h). The analysis of the MD trajectories shows that already at 500 K the oblate Au_{38t} structure completely loses its original shape; four Au–S bonds break (two between the Au_{23} core and S of the $Au_2(SCH_3)_3$ units, one between the Au_{23} core and S of the SCH_3 bridge, and one within the $Au_3(SCH_3)_4$ units (see Fig. S2 in Supplementary material), and a polymeric ring composed of $Au_{7-8}(SCH_3)_7$ starts to form as an extension of the remaining $Au_{31-30}(SCH_3)_{17}$ fragment (Fig. 3c). Consequently, the $Au_7(SCH_3)_7$ ring detaches from the $Au_{31}(SCH_3)_{17}$ fragment when the temperature reaches 1000 K (Fig. 3d). After detachment, only a weak bonding energy of 0.31 eV is seen between the $Au_{31}(SCH_3)_{17}$ and $Au_7(SCH_3)_7$ fragments, which was obtained from PBE calculations as $E([Au_{31}(SCH_3)_{17}]^0) + E([Au_7(SCH_3)_7]^0) - E([Au_{38}(SCH_3)_{24}]^0)$. On the other hand, the Au_{38q} cluster remains robust within a temperature range of 0–800 K (see Figs. 3f–3g) and Au–S bonds break only when the temperature exceeds 800 K (see Figs. 3g–3h and Fig. S2 in Supplementary material). Here it is important to point out that the temperature of fragmentation that could be measured experimentally might significantly differ from the values reported here since all the stabilizations arising from the ligands (such as ligand–ligand interactions and steric effects) have been omitted for practical purposes. Moreover, and despite the large number of observations of core-size conversion of MPC upon ligand exchange under heating [14,49–51], to the best of our knowledge there are not reports on the fragmentation of this type of systems caused solely by the effect of temperature. In addition, modeling the time scales involve in the fragmentation of MPC at room temperature is unfeasible by using ab initio calculations.

Figure 4 shows the evolution of the geometric structure of Au_{38t} and Au_{38q} clusters throughout the molecular dynamics simulation; the evolution of the three Cartesian moments of inertia (Figs. 4b and 4f), the evolution of the averaged Au–S bond distances (Figs. 4c and 4g), and the root mean square displacement (RMSD) of the Au atoms of the Au_{23} core and units (Figs. 4d and 4h) as a function of time. Figures 4b and 4f show that while the deformation of the oblate Au_{38t} cluster into an almost-prolate one occurs already when the system reaches 500 K (∼3.70 ps), the Au_{38q} cluster remains close to the original prolate throughout the simulation. The averaged Au–S distances plotted along the simulations in Figures 4c and 4g are measured using as reference the original Au–S bonding as assigned in the optimized Au_{38t} and Au_{38q} structures displayed in Figures 3a and 3e. The evolution of the averaged Au–S distances shows that the bonds between Au atoms of the Au_{23} core and S atoms (Au_{core}–S) are more susceptible to break than the Au–S bonds within the protecting
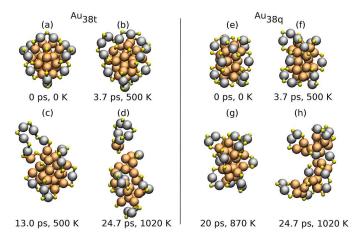

Fig. 3. Snapshots of the $Au_{38}(SCH_3)_{24}$ structures of Tian (Au_{38t}) and Qian (Au_{38q}) taken during the MD simulations using a time step of 2fs. Based on the initial disposition of Au and S atoms in the optimized Au_{38t} (a) and Au_{38q} (e) structures, the fifteen Au atoms of the original $Au_n(SCH_3)_m$ units and the twenty-three Au atoms of the initial Au_{23} core are depicted in gray and orange, respectively. Similarly, the bonds between the atoms of the original Au_{23} core and the S atoms (Au_{core}–S), and the Au–S bonds within the $Au_n(SCH_3)_m$ units (Au_{units}–S) are in orange and in gray, respectively. The S atoms are in yellow, and the CH_3 groups are not displayed to facilitate visualization. Time and temperature are given below each snapshot.

units (Au_{units}–S). Particularly, the first bonds to break are the ones between the Au_{23} core and S atoms of the $Au_2(SCH_3)_3$ units. This was also observed in the simulations of Au_{38t} performed using a time step of 1 fs (see Fig. S4 in Supplementary material). Moreover, the RMSD plots of Au_{38t} show that the 15 Au atoms of the original the protecting $Au_{15}(SCH_3)_{24}$ layer have larger RMSD values throughout the MD run than the 23 Au atoms in the original core. The same is true for the Au_{38q} structure but, in general, the RMSD values of all Au atoms in the Au_{38q} structure are significantly smaller than the ones calculated for Au_{38t}. The foregoing demonstrates the weakness of the Au_{core}–S bonds and the higher fluxionality of the Au atoms in the Au_{38t} structure compared to Au_{38q}. Moreover, in both structures the almost-completed closure of the HOMO–LUMO energy gap was observed once the temperature reached 1000 K (see Fig. S5 in Supplementary material).

4 Concluding remarks

We present a theoretical analysis of stability and robustness of two well-known ligand protected metal nanoclusters synthesized independently by Tian [34] and Qian [33]. These nanoclusters, which chemical formula is $Au_{38}(SCH_2CH_2Ph)_{24}$, have been found to have either an oblate (Au_{38T}) or a prolate (Au_{38Q}) shape depending on the synthesis conditions. Using different approximations to the exchange-correlation functional in DFT calculations we found that these two isomers are separated by
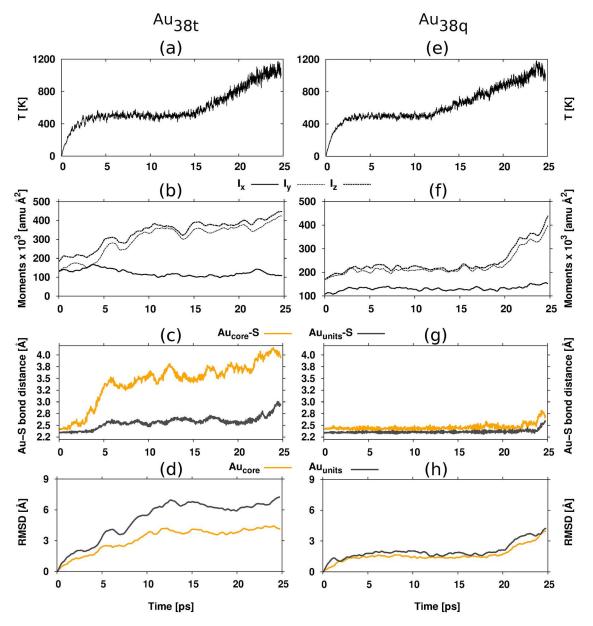
Fig. 4. Time evolution of temperature (a, e), moments of inertia (b, f), averaged Au–S bond distances (c, g), and root mean square displacement of Au atoms (d, h) of the structures Au_{38t} (a–d) and Au_{38q} (e–h) taken during the MD simulations. In (b) and (f) the moments of inertia are represented by I_x, I_y and I_z. In (c) and (g) the evolution of the averaged Au_{core}–S (orange) and Au_{units}–S (gray) distances are measured using as reference the original bonding as it is in the optimized atomic structures. In (d) and (h) the RMSD of the 15 and 23 Au atoms of the original units and core are in gray and orange, respectively.

an energy of 1.8–3.1 eV per cluster, Au_{38Q} being the more stable. Moreover, the energy difference between the two isomers is the largest when the vdW interactions are considered. Hence, when the SCH_2CH_2Ph ligands are replaced by SCH_3 the energy difference between the two isomers significantly drops (by up to 80–85%), indicating that large part of the stability of the Au_{38Q} structure arises from the disposition of the ligands around the prolate core. Furthermore, we found that the energy difference between the two $Au_{38}(SR)_{24}$ isomers (in eV per atom) is of the same order of magnitude as the energy difference between the *fcc* and *hcp* phases of bulk

gold calculated earlier using the DFT/PW91 level of theory [44].

In addition, the results from the MD simulations performed on the $Au_{38}(SCH_3)_{24}$ models demonstrate that while under the exposure of high temperatures (<800 K) the structure of Qian remains robust, the oblate structure of Tian undergoes drastic structural changes driven by a combined effect of high fluxionality of Au atoms and the weakness of the Au–S bonds between the Au_{23} core and the S atoms of the units. Hence, these results offer a qualitative comparison of the robustness of the thiolate-protected Au_{38} structure in the two geometric

arrangements, at the same time that they propose a possible decomposition mechanism of passivated-gold systems under heating via formation and detachment of $Au_x(SR)_y$ polymeric chains.

Author contribution statement

R.J.M. designed, performed the simulations, and wrote the manuscript. S.M. gave assistance and guidance in the analysis of the MD simulations. H.H. gave the suggestions and discussions. All authors contributed in editing the manuscript.

References

1. M. Brust, M. Walker, D. Bethell, D.J. Schiffrin, R. Whyman, J. Chem. Soc. Chem. Commun. **7**, 801 (1994)
2. R.L. Whetten, J.T. Khoury, M.M. Alvarez, S. Murthy, I. Vezmar, Z.L. Wang, P.W. Stephens, C.L. Cleveland, W.D. Luedtke, U. Landman, Adv. Mater. **8**, 428 (1996)
3. M.M. Alvarez, J.T. Khoury, T.G. Schaaff, M. Shafigullin, I. Vezmar, R.L. Whetten, Chem. Phys. Lett. **266**, 91 (1997)
4. T.G. Schaaff, M.N. Shafigullin, J.T. Khoury, I. Vezmar, R.L. Whetten, W.G. Cullen, P.N. First, C. Gutiérrez-Wing, J. Ascensio, M.J. Jose-Yacamán, J. Phys. Chem. B **101**, 7885 (1997)
5. T. Tsukuda, H. Häkkinen, *Protected Metal Clusters: From Fundamentals to Applications*, edited by T. Tsukuda, H. Häkkinen, 1st edn. (Elsevier, Amsterdam, 2015)
6. R. Jin, C. Zeng, M. Zhou, Y. Chen, Chem. Rev. **116**, 10346 (2016)
7. R. Jin, Nanoscale **7**, 1549 (2015)
8. I. Chakraborty, T. Pradeep, Chem. Rev. **117**, 8208 (2017)
9. B. Zhang, G. Salassa, T. Burgi, Chem. Commun. **52**, 9205 (2016)
10. T. Burgi, Nanoscale **7**, 15553 (2015)
11. S. Knoppe, I. Dolamic, T. Bürgi, J. Am. Chem. Soc. **134**, 13114 (2012)
12. K.R. Krishnadas, A. Baksi, A. Ghosh, G. Natarajan, A. Som, T. Pradeep, Acc. Chem. Res. **50**, 1988 (2017)
13. A. Ghosh, D. Ghosh, E. Khatun, P. Chakraborty, T. Pradeep, Nanoscale **9**, 1068 (2017)
14. M. Rambukwella, L. Sementa, A. Fortunelli, A. Dass, J. Phys. Chem. C **121**, 14929 (2017)
15. J. Jung, S. Kang, Y.-K. Han, Nanoscale **4**, 4206 (2012)
16. L.D. Marks, Rep. Prog. Phys. **57**, 603 (1994)
17. T. Ben-David, Y. Lereah, G. Deutscher, J.M. Penisson, A. Bourret, R. Kofman, P. Cheyssac, Phys. Rev. Lett. **78**, 2585 (1997)
18. D. Smith, A.K. Petford-long, L.R. Wallenberg, J.O. Bovin, Science **233**, 872 (1986)
19. S. Iijima, T. Ichihashi, Phys. Rev. Lett. **56**, 616 (1986)
20. Z.W. Wang, R.E. Palmer, Phys. Rev. Lett. **108**, 245502 (2012)
21. Z.Y. Li, N.P. Young, M. Di Vece, S. Palomba, R.E. Palmer, A.L. Bleloch, B.C. Curley, R.L. Johnston, J. Jiang, J. Yuan, Nature **451**, 46 (2008)
22. M. Azubel, A.L. Koh, K. Koyasu, T. Tsukuda, R.D. Kornberg, ACS Nano **11**, 11866 (2017)
23. M. Azubel, J. Koivisto, S. Malola, D. Bushnell, G.L. Hura, A.L. Koh, H. Tsunoyama, T. Tsukuda, M. Pettersson, H. Häkkinen, R.D. Kornberg, Science **345**, 909 (2014)
24. W. Chen, S. Chen, *Functional Nanometer-Sized Clusters of Transition Metals*, edited by W. Chen, S. Chen, 1st edn. (The Royal Society of Chemistry, 2014)
25. K.M.Ø. Jensen, P. Juhas, M.A. Tofanelli, C.L. Heinecke, G. Vaughan, C.J. Ackerson, S.J.L. Billinge, Nat. Commun. **7**, 11859 (2016)
26. H. Häkkinen, R.N. Barnett, U. Landman, Phys. Rev. Lett. **82**, 3264 (1999)
27. I.L. Garzón, C. Rovira, K. Michaelian, M.R. Beltrán, P. Ordejón, J. Junquera, D. Sánchez-Portal, E. Artacho, J.M. Soler, Phys. Rev. Lett. **85**, 5250 (2000)
28. I.L. Garzón, K. Michaelian, M.R. Beltrán, A. Posada-Amarillas, P. Ordejón, E. Artacho, D. Sánchez-Portal, J.M. Soler, Eur. Phys. J. D **9**, 211 (1999)
29. Y. Pei, Y. Gao, X.C. Zeng, J. Am. Chem. Soc. **130**, 7830 (2008)
30. H. Häkkinen, M. Walter, H. Grönbeck, J. Phys. Chem. B **110**, 9927 (2006)
31. O. Lopez-Acevedo, H. Tsunoyama, T. Tsukuda, H. Häkkinen, C.M. Aikens, J. Am. Chem. Soc. **132**, 8210 (2010)
32. D. Jiang, W. Luo, M.L. Tiago, S. Dai, J. Phys. Chem. C **112**, 13905 (2008)
33. H. Qian, W.T. Eckenhoff, Y. Zhu, T. Pintauer, R. Jin, J. Am. Chem. Soc. **132**, 8280 (2010)
34. S. Tian, Y.-Z. Li, M.-B. Li, J. Yuan, J. Yang, Z. Wu, R. Jin, Nat. Commun. **6**, 8667 (2015)
35. H. Mäkinen, V. Häkkinen, Eur. Phys. J. D **66**, 310 (2012)
36. J. Enkovaara, C. Rostgaard, J.J. Mortensen, J. Chen, M. Dulak, L. Ferrighi, J. Gavnholt, C. Glinsvad, V. Haikola, H.A. Hansen, H.H. Kristoffersen, M. Kuisma, A.H. Larsen, L. Lehtovaara, M. Ljungberg, O. Lopez-Acevedo, P.G. Moses, J. Ojanen, T. Olsen, V. Petzold, N.A. Romero, J. Stausholm-Møller, M. Strange, G.A. Tritsaris, M. Vanin, M. Walter, B. Hammer, H. Häkkinen, G.K.H. Madsen, R.M. Nieminen, J.K. Nørskov, M. Puska, T.T. Rantala, J. Schiøtz, K.S. Thygesen, K.W. Jacobsen, J. Phys.: Condens. Matter **22**, 253202 (2010)
37. J.J. Mortensen, L.B. Hansen, K.W. Jacobsen, Phys. Rev. B **71**, 35109 (2005)
38. J.P. Perdew, Y. Wang, Phys. Rev. B **45**, 13244 (1992)
39. J.P. Perdew, K. Burke, M. Ernzerhof, Phys. Rev. Lett. **77**, 3865 (1996)
40. K. Berland, P. Hyldgaard, Phys. Rev. B **89**, 35412 (2014)
41. A.H. Larsen, M. Kuisma, J. Löfgren, Y. Pouillon, P. Erhart, P. Hyldgaard, Model. Simul. Mater. Sci. Eng. **25**, 65004 (2017)

42. H.J.C. Berendsen, J.P.M. Postma, W.F. van Gunsteren, A. DiNola, J.R. Haak, J. Chem. Phys. **81**, 3684 (1984)
43. M. Walter, J. Akola, O. Lopez-Acevedo, P.D. Jadzinsky, G. Calero, C.J. Ackerson, R.L. Whetten, H. Grönbeck, H. Häkkinen, Proc. Natl. Acad. Sci. USA **105**, 9157 (2008)
44. C. Wang, H. Wang, T. Huang, X. Xue, F. Qiu, Q. Jiang, Sci. Rep. **5**, 10213 (2015)
45. X. Huang, S. Li, Y. Huang, S. Wu, X. Zhou, S. Li, C.L. Gan, F. Boey, C.A. Mirkin, H. Zhang, Nat. Commun. **2**, 292 (2011)
46. H. Qian, Y. Zhu, R. Jin, ACS Nano **3**, 3795 (2009)
47. B.M. Quinn, P. Liljeroth, V. Ruiz, T. Laaksonen, K. Kontturi, J. Am. Chem. Soc. **125**, 6644 (2003)
48. O. Toikkanen, V. Ruiz, G. Rönnholm, N. Kalkkinen, P. Liljeroth, B.M. Quinn, J. Am. Chem. Soc. **130**, 11049 (2008)
49. P.R. Nimmala, S. Theivendran, G. Barcaro, L. Sementa, C. Kumara, V.R. Jupally, E. Apra, M. Stener, A. Fortunelli, A. Dass, J. Phys. Chem. Lett. **6**, 2134 (2015)
50. C. Zeng, C. Liu, Y. Pei, R. Jin, ACS Nano **7**, 6138 (2013)
51. C. Zeng, H. Qian, T. Li, G. Li, N.L. Rosi, B. Yoon, R.N. Barnett, R.L. Whetten, U. Landman, R. Jin, Angew. Chemie Int. Ed. **51**, 13114 (2012)